Nuclear shell effects near the *r*-process path in the relativistic Hartree-Bogoliubov theory

Madan M. Sharma and Ameena R. Farhan

Physics Department, Kuwait University, Safat, Kuwait 13060

We have investigated the evolution of the shell structure of nuclei in going from the *r*-process path to the neutron drip line within the framework of the relativistic Hartree-Bogoliubov (RHB) theory. By introducing the quartic self-coupling of ω meson in the RHB theory in addition to the nonlinear scalar coupling of σ meson, we reproduce the available data on the shell effects about the waiting-point nucleus ^{80}Zn. With this approach, it is shown that the shell effects at $N=82$ in the inaccessible region of the *r*-process path become milder as compared to the Lagrangian with the scalar self-coupling only. However, the shell effects remain stronger as compared to the quenching exhibited by the HFB+SkP approach. It is also shown that in reaching out to the extreme point at the neutron drip line, a terminal situation arises where the shell structure at the magic number is washed out significantly.

I. INTRODUCTION

A knowledge of the shell effects near the *r*-process path is important for discerning the astrophysical scenario of nucleosynthesis [1]. The question whether the shell effects near the drip lines are strong or do quench has become crucial to understanding the nucleosynthesis of heavy nuclei. The $N=82$ nuclei at the *r*-process path are assumed to play a significant role in providing nuclear abundances about $A\sim130$. Since nuclei contributing to this peak are extremely neutron-rich and are not accessible experimentally, it has not been possible to ascertain the nature of the shell effects in the vicinity of the *r*-process path. Due to the lack of experimental data, there prevail conflicting viewpoints [2,3] on the strength of the shell effects near the *r*-process path.

In Ref. [2] the shell effects in the region of the *r*-process path at $N=82$ were studied on the basis of the relativistic mean-field (RMF) theory using a successful nuclear interaction. It was predicted [2] that the shell effects at $N=82$ in Zr nuclei are strong. In contrast, the shell effects were suggested [3] to be quenched on the basis of the Hartree-Fock-Bogoliubov (HFB) calculations using the density-dependent Skyrme force SkP. In the absence of experimental data on the shell effects for $N=82$ nuclei near the *r*-process path, however, it is difficult to verify either of the two predictions. In view of this, we first attempt to reproduce the available data on the shell effects in the known regions and then extrapolate the method to the inaccessible region.

In this paper, we examine how the shell effects evolve with isospin in the region of the astrophysically important magic number $N=82$ near the *r*-process path. Using the experimental data available on the waiting-point nucleus ^{80}Zn $(N=50)$, we explore the shell effects near the *r*-process path in the framework of the relativistic Hartree-Bogoliubov (RHB) theory with the self-consistent finite-range pairing. In order to improve the description of the shell effects, we have also introduced the vector self-coupling of ω meson in addition to the nonlinear scalar coupling of the σ meson in the RHB theory. It has been shown that with this approach the high-precision experimental data on the shell

effects about the stability line can be reproduced well [4]. This forms our basis to be able to predict how the shell effects evolve in the unknown region.

The shell effects are known to manifest strongly in terms of the magic numbers. This is signified by a prominent kink about the major magic numbers as can be seen vividly in the two-neutron separation energies (S_{2n}) all over the periodic table [5]. This is a demonstration of the existence of large shell gaps at magic numbers in nuclei about the stability line. Here the spin-orbit interaction is pivotal in the creation of the magic numbers [6]. In the RMF theory [7] the spin-orbit term arises naturally as a consequence of the Dirac-Lorentz structure of nucleons. This has shown much usefulness in explaining properties that involve shell effects such as anomalous isotope shifts in stable nuclei [8]. The form of the spin-orbit interaction in the RMF theory has been found to be advantageous over that in the nonrelativistic approaches [9].

For nuclei near the drip line, a coupling to the continuum is required. A self-consistent treatment of pairing is also desirable. The framework of the RHB theory provides an appropriate tool to include both these features. Thus, in the RHB theory the advantage of a relativistic description of the RMF approach in the Hartree channel is combined with that of a self-consistent finite-range pairing force. We provide a short summary of the RHB theory in the next section. In Sec. III we give the details of the calculations. The ensuing results are presented and discussed in Sec. IV. Here a detailed comparison of the shell effects using different forces and approaches is made. The single-particle levels are used to illustrate the nature of the shell effects in the different approaches. The last section concludes the results of the paper.

II. THE RELATIVISTIC HARTREE-BOGOLIUBOV THEORY

The RMF Lagrangian that describes the nucleons as Dirac spinors moving in meson fields is given by [7]

$$\mathcal{L} = \bar{\psi}\left(\not{p} - g_\omega\not{\omega} - g_\rho\vec{\not{\rho}}\vec{\tau} - \frac{1}{2}e(1-\tau_3)\not{A} - g_\sigma\sigma - M_N\right)\psi$$

$$+ \frac{1}{2}\partial_\mu\sigma\partial^\mu\sigma - U(\sigma) - \frac{1}{4}\Omega_{\mu\nu}\Omega^{\mu\nu} + \frac{1}{2}m_\omega^2\omega_\mu\omega^\mu$$

$$+ \frac{1}{2}g_4(\omega_\mu\omega^\mu)^2 - \frac{1}{4}\vec{R}_{\mu\nu}\vec{R}^{\mu\nu} + \frac{1}{2}m_\rho^2\vec{\rho}_\mu\vec{\rho}^\mu - \frac{1}{4}F_{\mu\nu}F^{\mu\nu}, \tag{1}$$

where M_N is the bare nucleon mass and ψ is its Dirac spinor. In addition, we have the scalar meson (σ), isoscalar vector meson (ω), isovector vector meson (ρ), and the electromagnetic field A^μ, with the masses m_σ, m_ω, and m_ρ and the coupling constants g_σ, g_ω, and g_ρ, respectively. The field tensors for the vector mesons are given as $\Omega_{\mu\nu} = \partial_\mu\omega_\nu - \partial_\nu\omega_\mu$ and by similar expressions for the ρ meson and the photon. For a realistic description of nuclear properties a nonlinear self-coupling $U(\sigma) = \frac{1}{2}m_\sigma^2\sigma^2 + \frac{1}{3}g_2\sigma^3 + \frac{1}{4}g_3\sigma^4$ for σ mesons has become standard. We have added the nonlinear vector self-coupling of a ω meson [10], which is represented by the coupling constant g_4.

Using Green's function techniques [11] it has been shown in Ref. [12] that a relativistic Hartree-Bogoliubov theory can be implemented using such a Lagrangian. Neglecting retardation effects one obtains relativistic Dirac-Hartree-Bogoliubov (RHB) equations

$$\begin{pmatrix} h & \Delta \\ -\Delta^* & -h^* \end{pmatrix}\begin{pmatrix} U \\ V \end{pmatrix}_k = E_k\begin{pmatrix} U \\ V \end{pmatrix}_k, \tag{2}$$

where E_k are the quasiparticle energies and the coefficients U_k and V_k are four-dimensional Dirac spinors normalized as

$$\int (U_k^\dagger U_{k'} + V_k^\dagger V_{k'})d^3r = \delta_{kk'}. \tag{3}$$

The average field

$$h = \boldsymbol{\alpha}\boldsymbol{p} + g_\omega\omega + \beta(M + g_\sigma\sigma) - \lambda \tag{4}$$

contains the chemical potential λ, which is adjusted to the proper particle number. The meson fields σ and ω are determined self-consistently from the Klein-Gordon equations:

$$\{-\Delta + m_\sigma^2\}\sigma = -g_\sigma\rho_s - g_2\sigma^2 - g_3\sigma^3, \tag{5}$$

$$\{-\Delta + m_\omega^2\}\omega = g_\omega\rho_v + g_4\omega^3, \tag{6}$$

with the scalar density $\rho_s = \Sigma_k\bar{V}_kV_k$ and the baryon density $\rho_v = \Sigma_k V_k^\dagger V_k$. The sum on k runs only over all the particle states in the *no-sea* approximation. The pairing field Δ in Eq. (2) is given by

$$\Delta_{ab} = \frac{1}{2}\sum_{cd} V_{abcd}^{pp}\kappa_{cd}, \tag{7}$$

where V_{abcd}^{pp} are the matrix elements of a general two-body pairing interaction, and the pairing tensor is defined as

$$\kappa_{cd}(\mathbf{r},\mathbf{r}') = \sum_{E_k>0} U_{ck}^*(\mathbf{r})V_{dk}(\mathbf{r}'). \tag{8}$$

The RHB equations (2) are a set of four coupled integrodifferential equations for the Dirac spinors $U(r)$ and $V(r)$ that are obtained self-consistently. The solution of the Dirac-Hartree-Bogoliubov eigenvalue equations and the meson-field equations determines the nuclear ground state.

Nuclei that are known to show strong pairing correlations are treated appropriately within the framework of the RHB approach. This is especially important when the pairing correlations in the middle of a shell become significant. On the other hand, the pairing correlations for nuclei of two neutrons less or more than a magic number can be expected to be similar in the RHB and the BCS approach. This is due to the reason that the pairing correlations in such nuclei are reduced to a minimal level. However, in the present work, we have performed the RHB calculations for all nuclei. For the pairing channel, we have taken the finite-range Gogny force D1S. It is known to represent the pairing properties of a large number of finite nuclei appropriately [13].

The RHB approach becomes important while dealing with nuclei far away from the stability line and in particular for those in the vicinity of the drip lines where the Fermi level is usually very close to the continuum. The RHB theory, which is based upon the quasiparticle scheme employing Bogoliubov transformations, takes into account the coupling between the bound states and the states in the continuum. The pairing and the coupling to the continuum can be important in nuclei with a pair of particles above the shell closure in determining the shell effects especially as the Fermi surface is very close to the continuum. Therefore, the RHB theory with the self-consistent pairing serves as an ideal scheme for this purpose.

III. DETAILS OF THE CALCULATIONS

The RHB calculations have been performed for nuclei in the neighborhood of the waiting-point Zn nuclei and for nuclei from r-process path to the neutron drip line. Nuclei are treated within a spherically symmetric configuration. The method of expansion of the wave functions into the harmonic oscillator basis is employed [14]. We have taken 20 shells both for the fermionic as well as bosonic wave functions for the expansion.

A comparative study is made between the Lagrangian model with the nonlinear scalar self-coupling of the σ meson and the Lagrangian with both the nonlinear scalar self-coupling of the σ and the vector self-coupling of the ω meson. For the former, we have used the force NL-SH, which is a typical representative for this Lagrangian model. In a large number of studies it has been shown that the force NL-SH [15] is able to provide a very good description of the ground-state properties of nuclei all over the periodic table. It has been found to be especially useful for exotic nuclei near the drip lines. Recently, the force NL3 [16] has been brought out with a view to improve the description of the giant monopole resonance. However, as shown in Ref. [4] ground-state properties of nuclei predicted by NL3 are very similar to those of NL-SH.

For the Lagrangian with the nonlinear vector self-coupling of the ω meson, which is in addition to the usual nonlinear scalar self-coupling of the σ meson, we have used the forces NL-SV1 and NL-SV2. These forces have been developed recently [4,17] with a view to bring about an improvement in the ground-state properties of nuclei *vis-à-vis* the scalar self-coupling. Consequently, it has been shown by Sharma *et al.* [4] that the introduction of the vector self-coupling was a remedial measure with respect to the shell effects in nuclei about the stability line. In addition, the high-density equation of state (EOS) of the nuclear matter becomes softer as compared to that with the scalar self-coupling only. This would make the Lagrangian model with the vector self-coupling compatible with the neutron star masses. The detailed properties of these forces will be provided elsewhere [17].

IV. RESULTS AND DISCUSSION

In our attempt to scrutinize the shell effects, we started our investigation [4] of the shell effects in nuclei at the stability line, where we examined the role of σ- and ω-meson couplings on the shell effects in Ni and Sn isotopes. It was observed that the existing nuclear forces based upon the nonlinear scalar self-coupling of σ-meson exhibit shell effects that were stronger than suggested by the experimental data. In order to remedy this problem, the nonlinear vector self-coupling of the ω meson in the RHB theory was introduced. As a result of this, the experimental data on the shell effects in Ni and Sn nuclei on the stability line were reproduced well [4].

A. The Zn nuclei near $N=50$

Having established the functional basis, we consider nuclei around ^{80}Zn ($N=50$) in the present work. The isotope ^{80}Zn is assumed to be a waiting-point nucleus in the chain of *r*-process nucleosynthesis and comes closest to the β-stability line for nuclei with $N=50$. The experimental S_{2n} value for this nucleus is about 11 MeV. The nuclei ^{80}Zn and ^{82}Zn, being very rich in neutrons, would serve to test the theoretical models far away from the stability line. Here, we present the results on the shell effects in the waiting-point Zn nuclei about $N=50$ using different model Lagrangians. The S_{2n} values for the Zn isotopes obtained from the RHB calculations are shown in Fig. 1. The experimental data are taken from the 1995 mass tables [18]. Because the mass of the nucleus ^{82}Zn is based upon the systematics, there may be a slight uncertainty in the S_{2n} value of the nucleus ^{82}Zn. Thus, the data point for ^{82}Zn is shown in Fig. 1 enclosed within a diamond.

The RHB calculations [Fig. 1(a)] with NL-SH (scalar self-coupling only) show a very large kink at $N=50$ implying that the shell effects with NL-SH are much stronger than those exhibited by the available data. In comparison, the shell gap with NL-SV2 (both the scalar and vector self-couplings) is reduced as compared to NL-SH. It is, however, still larger than the data shown. The reduction in the shell gap with the vector self-coupling is consistent with that ob-
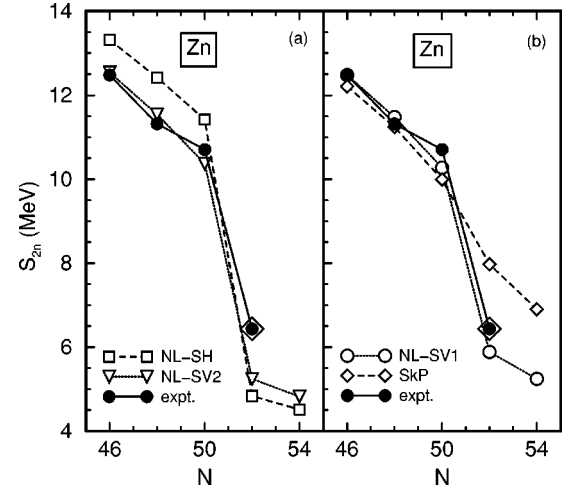

FIG. 1. The S_{2n} values for Zn isotopes in the waiting-point region obtained with RHB using (a) the scalar self-coupling force NL-SH and the vector self-coupling force NL-SV2 and (b) with the vector self-coupling force NL-SV1 along with the nonrelativistic HFB+SkP results. The experimental data are shown for comparison. The datum on ^{82}Zn is adopted from the mass systematics [18] and is shown enclosed within a diamond.

served in Ni nuclei at the stability line *vis-à-vis* the scalar self-coupling only.

We show in Fig. 1(b) the S_{2n} values obtained with the other vector self-coupling force NL-SV1. The slope of the kink shows that the shell gap with NL-SV1 agrees well with the available data. Thus, RHB with the vector self-coupling Lagrangian NL-SV1 is able to reproduce the available data on the shell effects in the waiting-point region satisfactorily. We also show in Fig. 1(b) the nonrelativistic HFB calculations with the Skyrme force SkP [19]. The SkP results produce nearly a straight line passing through the $N=50$ point. A comparison of these results with the data shows that the shell effects with SkP are quenched strongly. This is reminiscent of the behavior of SkP as observed in Ref. [4] at the stability line, where the shell effects were found to be quenched strongly in Ni isotopes at $N=28$ in contrast to the experimental data. This feature of SkP is evidently due to its high effective mass $m^* \sim 1$, which increases the level density near the Fermi surface and thus suppresses the shell gaps significantly [19].

B. Nuclei about $N=82$ near the *r*-process path

Nuclei in the vicinity of $Z=40$ with the magic neutron number $N=82$ are expected to lie on or close to the *r*-process path. We have chosen the isotopic chains $Z=36$ -46 with neutron numbers running across the magic number $N=82$. The *r*-process path is expected to pass through these nuclei, especially those with the higher Z values. Some nuclei in these chains are close to the neutron drip line as the neutron separation energy approaches a vanishing value.

How the shell effects behave in nuclei near the *r*-process path is an open question. This is due to the fact that the $N=82$ nuclei near the *r*-process path possess an extremely large neutron-to-proton ratio. Although tremendous progress
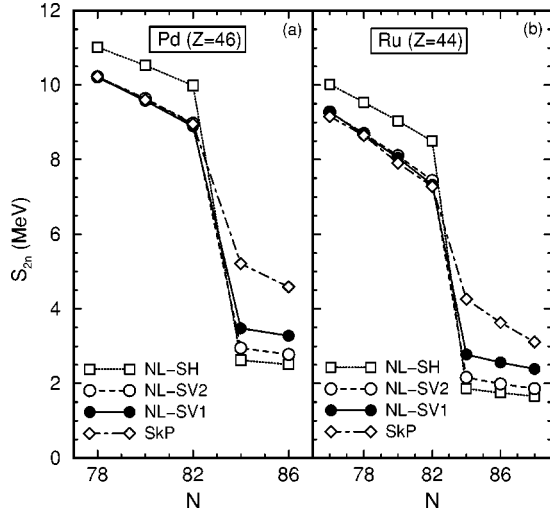
FIG. 2. The RHB results on the shell effects at $N = 82$ in the r-process nuclei of (a) Pd and (b) Ru. The HFB+SkP results are also shown for a comparison.

FIG. 3. The same as Fig. 2 for the r-process nuclei (a) Mo and (b) Zr. The S_{2n} values and shell gaps show a gradual decline in moving from Pd to Zr.

has been made in the last decade in synthesizing very-neutron-rich nuclei in the laboratory, such nuclei are still very far from being realized. The last such nucleus attained in this region in the laboratory is ^{130}Cd ($Z = 48$ and $N = 82$). The mass of the nucleus ^{132}Cd with $N = 84$ is still not known. Knowledge of the latter would allow us to discern the shell effects in regions far away from the stability line. For $N = 82$ nuclei with $Z < 48$, i.e., in the region of Zr ($Z = 40 - 44$), the magnitude of the nuclear isospin becomes increasingly large and hence the difficulty in producing these nuclei. In the present paper, we examine the shell effects in these nuclei, therefore, in the light of the data available in the other regions. We also study how the shell effects evolve as one approaches the continuum in moving from the r-process path towards the neutron drip line.

Having described the available data on the waiting-point Zn nuclei by the forces with the vector self-coupling as shown in Fig. 1, we extend our formalism to explore the inaccessible region of the r-process path and the neutron drip line about $N = 82$. With a view to visualize the evolution of the shell effects with the isospin, we show our RHB results on the S_{2n} values for the isotopic chains from the higher Z to the lower ones using the two Lagrangian models. Figure 2 shows the corresponding values for the Pd ($Z = 46$) and Ru ($Z = 44$) nuclei across the magic number $N = 82$.

The results (Fig. 2) with the nonlinear scalar self-coupling (NL-SH) for the Pd and Ru isotopic chains show a shell gap at $N = 82$, which is largest among all the forces shown here. With the force NL-SV2 with the vector self-coupling of the ω meson, the shell effects are milder as compared to NL-SH. This feature is similar to that observed at the stability line [4] and also in Fig. 1. Furthermore, the results with the force NL-SV1 show that the shell gap at $N = 82$ is reduced as compared to NL-SV2. This is again similar to that seen for the Zn isotopes. For comparison, we also show the HFB results obtained with the interaction SkP. The shell gap with SkP is much reduced as compared to the forces with the vector self-coupling. Thus, the shell effects with NL-SV1 are
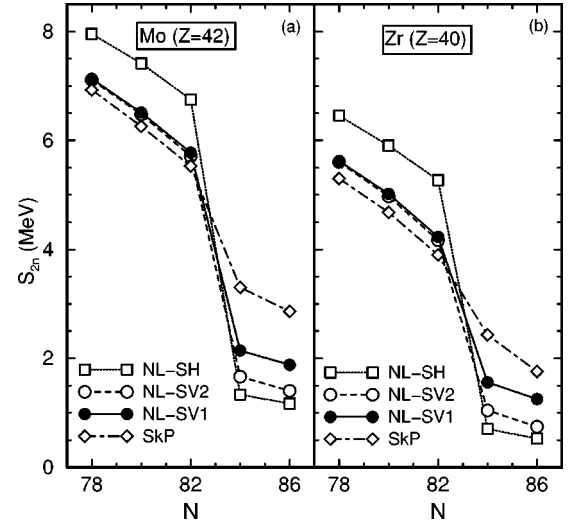
stronger as compared to the HFB+SkP results shown in the figure. It is interesting to note that there is a remarkable agreement in the results below and up to the magic number for all the forces except for NL-SH. The neutron separation energy from these results for $N = 82$ Pd and Ru nuclei is about $3 - 4$ MeV. Accordingly, these nuclei are expected to lie well on the r-process path as per the conventional wisdom.

We show the RHB results for the isotopic chains of Mo ($Z = 42$) and Zr ($Z = 40$) in Fig. 3. From the argument of the neutron separation energy, the Mo and Zr nuclei about the magic number are also expected to lie along the r-process path. Thus, both Figs. 2 and 3 portray how the shell effects evolve in moving to nuclei with larger neutron excess. The main feature that the shell effects with NL-SH are strong, is also displayed by Fig. 3. It is worth remembering that the force NL-SH was also used in an earlier work [2] to calculate the shell effects at $N = 82$ in Zr nuclei about the drip line. The shell effects with NL-SH were noted to be similarly strong in the previous results. However, the previous results with NL-SH were based upon the BCS pairing, and there was no mechanism in place to include the effects of the coupling to the continuum. The qualitative behavior that the shell effects with NL-SH are strong is reproduced here also in the present RHB calculations. The reason for this overestimation of the shell effects as also noted in Ref. [4] is that the properties that were considered mainly in constructing these forces such as NL-SH and others were the binding energies and charge radii of nuclei. The shell effects as such were not included in such considerations heretofore. As shown in Ref. [4], the shell effects emerge as an observable that should be employed to constrain the nuclear interaction.

With the force NL-SV2 with the vector self-coupling of the ω meson, the shell effects (Figs. 2 and 3) are milder as compared to NL-SH for all the chains. This is similar to that observed at the stability line [4] and also in Fig. 1(a). The results with our benchmark force NL-SV1 show that the shell gap at $N = 82$ is reduced as compared to NL-SV2. This is again similar to that observed for the Zn isotopes. The S_{2n}

values obtained with the HFB calculations using the Skyrme interaction SkP are also shown for comparison. The magnitude of the kink at $N=82$ shows that the shell effects with HFB+SkP are much weaker as compared to NL-SV1. The quenching predicted by SkP in this region is as expected. As noted earlier, HFB+SkP is known to exhibit a strong quenching at the stability line [4] and the same has also been observed about the waiting-point nucleus ^{80}Zn as shown in Fig. 1(b) above. In comparison, the RHB approach with NL-SV1 reproduces the shell effects about the stability line [4] as well as in the waiting-point region at $N=50$.

For any given force, the shell gap at $N=82$ shows a steady decrease in moving from Pd ($Z=46$) to Zr ($Z=40$). As nuclei become increasingly neutron-rich, the gradual decrease in the S_{2n} values and also in the corresponding shell gap shows the evolution of the shell effects in going away from the *r*-process path towards the drip line. This reduction in the shell gap is largest for SkP, which shows intrinsically weaker shell effects. As seen from Fig. 3(b) for the Zr isotopes, the curve for S_{2n} has become nearly a straight line, implying a disappearance of the magicity with SkP. This picture is at variance with that from NL-SV1. The persistence of the kink with NL-SV1 in Figs. 2 and 3 shows that with NL-SV1 the shell effects for the *r*-process nuclei at $N=82$ are much stronger than those with SkP. Thus, notwithstanding the fact that NL-SV1 is commensurate with the available data along the stability line and in the waiting-point region, it can be stated that the shell effects in $N=82$ nuclei on the *r*-process path still remain stronger.

C. Nuclei near the neutron drip line

Nuclei become increasingly unbound and a coupling to the continuum arises in going to extremely large neutron to proton ratios. This situation is expected to arise naturally in going to $N=82$ nuclei below $Z=40$. For this situation, we show the results for Sr ($Z=38$) and Kr ($Z=36$) isotopes in Fig. 4. The results show that the S_{2n} value for the $N=82$ nuclei decreases from ~ 2.5 MeV for Sr isotopes to ~ 1.5 MeV. The corresponding S_n value would amount to a merely 1 MeV or less. On the basis of the S_n, the $N=82$ Kr nucleus represents the arrival of the drip line.

The shell effects with NL-SV1 are seen to become successively weaker (which is true for all the forces) as one moves to nuclei with higher isospin such as ^{120}Sr [Fig. 4(a)] and ^{118}Kr [Fig. 4(b)]. Here, the case of the Kr isotopes [Fig. 4(b)] deserves mention. Except for NL-SH, all other forces show that the shell effects are washed out significantly. This stems from the fact that for ^{118}Kr the Fermi energy is very close to the continuum and the nucleus is pushed to the very limit of binding. The binding energy of an additional neutron is then close to zero and the shell gap ceases to exist. Thus, any semblance of the shell effects for ^{118}Kr ($N=82$) is completely lost. This situation is destined to befall on a nucleus or nuclei for every magic number, leading to a termination of the corresponding shell gap. All the forces NL-SV2, NL-SV1, and SkP predict such behavior except NL-
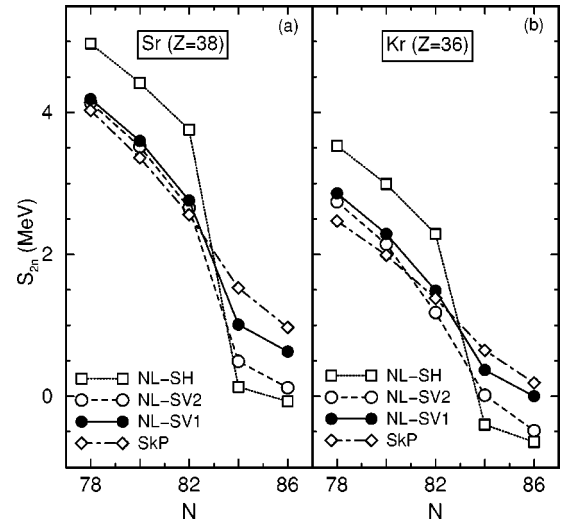

FIG. 4. The same as Fig. 2 for the drip-line nuclei near $N=82$ for the Sr and Kr isotopic chains. The shell gap and the S_{2n} values show a vanishing trend for the Kr isotopes about $N=82$.

SH. This situation at the drip line at the magic number can be termed as *terminus stratum*.

The nuclei close to the drip line show no binding to an extra neutron to be able to form a higher mass isotope. Such nuclei at the drip line ($\lambda_n \sim 0$) would not contribute to *r*-process nucleosynthesis. In view of this, it is therefore important to understand the nature of the shell effects for nuclei along the *r*-process path, which are assumed to play an important role in the nucleosynthesis, rather than those at the drip line.

D. The single-particle levels

We show in Fig. 5 the neutron single-particle levels obtained with NL-SV1 for $N=80$ nuclei from a few chains. Our focus is the evolution of the shell gap at $N=82$ as one approaches the drip line ($\lambda_n \sim 0$) from the *r*-process path. As discussed in the subsection above, the Mo and Zr nuclei are expected to lie on the *r*-process path, whereas the Sr and Kr nuclei should be very close to the drip line. The single-particle levels shown in this figure portray essentially the results of Figs. 3 and 4. The Fermi energy (shown by the dashed lines) approaches the continuum as one moves towards a larger neutron to proton ratio. The shell gap ($N=82$) shows a constant decrease as the last neutrons become more and more unbound in going from Mo to Kr. For ^{118}Kr ($N=82$) the Fermi energy is close to zero and the shell gap merges into the continuum. However, for nuclei on the *r*-process path such as Mo and Zr shell gaps do remain large. For the corresponding nuclei of Pd and Ru, the shell gaps are (not shown here) even larger than that for Mo.

The difference in the response of the various forces near the drip line is illustrated in the single-particle levels shown for ^{120}Zr in Fig. 6. Since this nucleus has two neutron less than the magic numbers, all the occupied levels are bound. Moreover, we do not see any indication of a partial occupancy of any level above the Fermi energy, which might arise from the Bogoliubov pairing. The figure shows that the
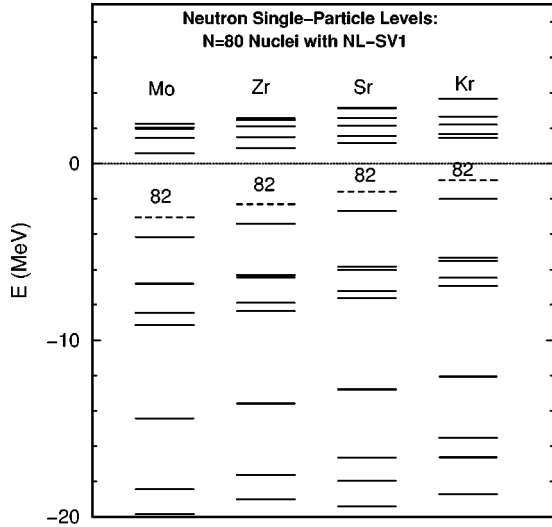
FIG. 5. The neutron single-particle levels for the Mo, Zr, Sr, and Kr nuclei ($N=80$) showing an evolution of the shell gap in moving from the r-process path towards the drip line, with the force NL-SV1. The Fermi energy is shown by the dashed lines. The Fermi energy for the Kr nucleus near the drip line is seen to merge with the continuum.

$N=82$ shell gap is largest with NL-SH and it shows a reduction in going to NL-SV1. This is consistent with the general behavior of the shell effects from NL-SH to NL-SV1 as seen in Figs. 2–4. On the other hand, the shell gap with SkP is reduced significantly as compared to NL-SV1. The reduced shell strength with SkP seems to be generic as shown above.

In Fig. 7 we have shown the neutron single-particle levels for the nucleus ^{124}Zr with two neutrons more than the magic number $N=82$. Here we have made a comparison of the levels for NL-SH, NL-SV1, and SkP. The shell gap at $N=82$ shows a decreasing trend from NL-SH to SkP as seen also in Fig. 6. However, it can be noticed that the extra two neutrons above the magic number go to the levels in the
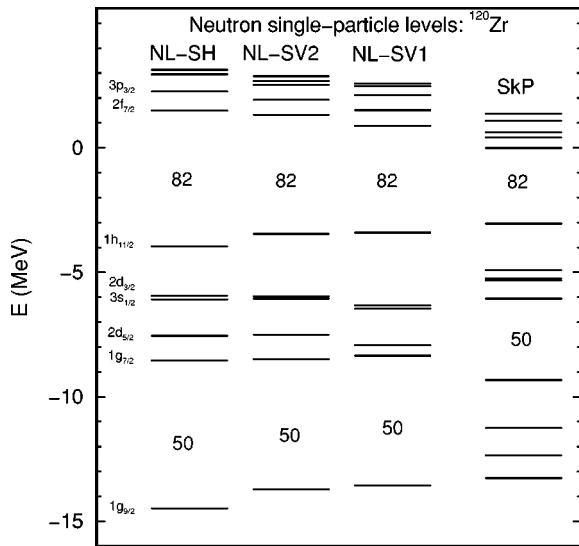

FIG. 6. The shell gap $N=82$ for the nucleus ^{120}Zr using the various interactions.
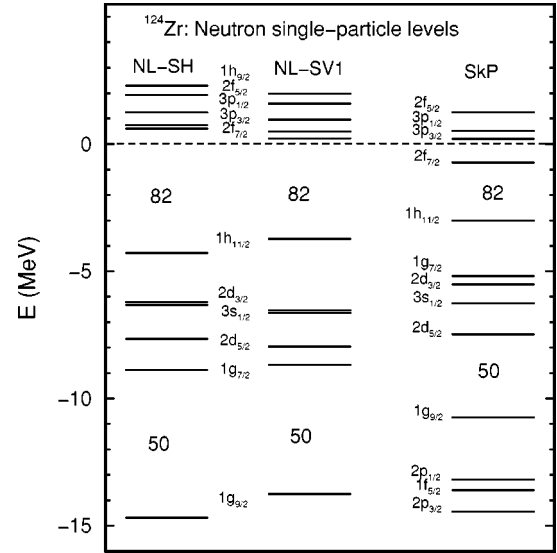

FIG. 7. The neutron single-particle levels for the nucleus ^{124}Zr with two neutrons above the closed shell. The reduction of the $N=82$ shell gap from NL-SH to NL-SV1 to SkP is clearly evident. In contrast to the RMF forces, the $2f_{7/2}$ level is bound with SkP.

continuum and therefore with the force NL-SH and NL-SV1 this nucleus is unbound. This should imply that ^{124}Zr is already a drip-line nucleus, whereas the same is not the case for ^{120}Zr (see Fig. 6). The single-particle levels with SkP show a remarkable difference from those of the RMF forces. With SkP the $2f_{7/2}$ level is below the continuum and the extra two neutrons occupy this level predominantly. Thus, the nucleus ^{124}Zr is bound within the HFB+SkP calculations in contrast to the RMF forces.

E. The spin-orbit potential

The spin-orbit potential is the key ingredient of the nuclear interaction responsible for creation of the magic numbers and the shell gaps. As mentioned earlier, the spin-orbit interaction arises naturally in the RMF theory as a result of the Dirac-Lorentz structure of nucleons. The σ and ω potentials contribute constructively to generate the required spin-orbit strength [7]. This is able to reproduce the experimental data on spin-orbit splittings in nuclei such as ^{16}O and ^{40}Ca. It has been shown by several authors [20,21] that the effective mass in the RMF theory can be constrained by the spin-orbit splittings in light nuclei to a value close to 0.60. However, the shell gaps and thus the shell effects in heavier nuclei cannot be addressed adequately by fixing the spin-orbit splittings in ^{16}O only. This becomes clear by examining the successful RMF forces such as NL-SH and NL3, which show stronger shell effects as compared to the experimental data in heavy nuclei [4]. This implies that the shell effects in heavier nuclei need to be taken into account in order to make a successful nuclear interaction. In this respect, the experimental data on S_{2n} values around the shell closure provide an additional useful ground-state observable.

The advantage that the RMF theory derives from its intrinsic spin-orbit interaction is not enjoyed by the nonrelativistic approaches such as the Hartree-Fock Skyrme theories.
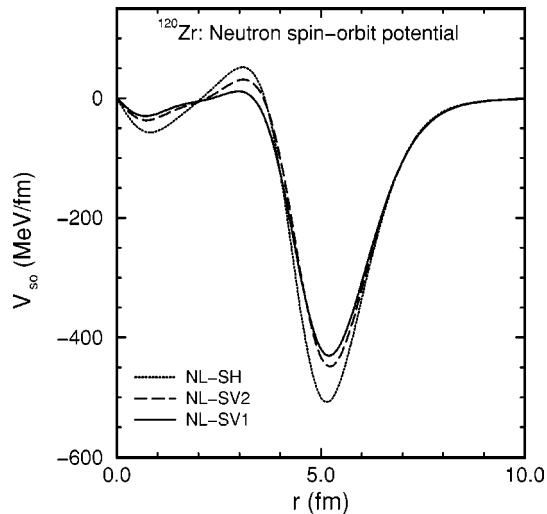
FIG. 8. The neutron spin-orbit potential for ^{120}Zn obtained in the RHB calculations with the various RMF forces. The predominance of the spin-orbit potential in the surface region is clearly evident.

The spin-orbit potential is usually added on an ad-hoc basis and the strength of the spin-orbit potential is fitted in order to reproduce the spin-orbit splittings in light nuclei in these approaches. This may, however, not suffice for the shell effects in heavy nuclei as illustrated for the case of the RMF theory.

The spin-orbit (s.o.) potential plays a central role in determining the magnitude of the spin-orbit splittings in nuclei. We show in Fig. 8 the spin-orbit potential obtained in the RHB theory for the Lagrangian parameters NL-SH, NL-SV2, and NL-SV1. The contribution of the σ and ω terms add together to give rise to the spin-orbit potential, which is predominant in the surface region of the nucleus [7]. The s.o. potential is largest for the nonlinear scalar force NL-SH. This is consistent with the strong shell effects observed with NL-SH at the shell closures in nuclei. The depth of the s.o. potential is reduced by about 10% for the force NL-SV2. It is reduced further with NL-SV1. This reduction from NL-SH to NL-SV2 and to NL-SV1 is consistent with all the results we have discussed on the shell effects with these forces in this work. This underlines the point that the spin-orbit interaction plays a key role in determining the strength of the shell effects. This would require an adjustment of both the σ and the ω fields in order to produce a suitable spin-orbit field.

V. CONCLUSION

We have investigated the evolution of the shell effects in nuclei from the r-process path to the neutron drip line. The theoretical approach that is employed in the present work is that of the relativistic Hartree-Bogoliubov theory based upon the quasiparticle scheme with the self-consistent pairing. The RHB approach with the inclusion of the vector self-coupling of ω meson was developed with a view to remedy the problem of the strong shell effects with the Lagrangian with the scalar self-coupling only. Having reproduced the shell effects with the vector self-coupling at the stability line in our earlier work [4], we have attempted to reproduce the available data on the shell effects in the waiting-point region of ^{80}Zn. The available data on Zn isotopes are reproduced well within the RHB approach with the vector self-coupling. This establishes further the reliability of the working basis we employ.

With the above approach we have carried out the RHB calculations for nuclei along the r-process path and near the neutron drip line using the two different Lagrangian models. It is shown that the shell effects with vector self-coupling are in general softer than those with the scalar self-coupling. This is found to be the case over a broad range of nuclei considered in our work. This implies that the shell structure near the Fermi surface with the vector self-coupling forces is denser than with the Lagrangian with the scalar self-coupling. This is consistent with what was found to be the case also for nuclei about the stability line.

The shell gap at $N=82$ shows a gradual decrease in going from the r-process path towards the neutron drip line for all the forces considered. This is the natural behavior for the shell gaps to evolve with the isospin. However, we show that for nuclei on the r-process path, the shell effects at $N=82$ still remain strong *vis-à-vis* a quenching exhibited by HFB $+$SkP. This quenching with SkP has been discussed extensively in the literature [1,3,22]. The origin of the shell quenching stems primarily from the very large effective mass of SkP, which leads to a significant compression of the shell structure near the Fermi surface. Quenching has been requested for an improved fit to the global r-process abundances [1,22]. However, quenching does not seem not to be compatible with the data at the stability line and in the waiting-point region.

In moving away from the r-process path where nuclei are expected to have $S_n \sim 2-4$ MeV to nuclei where S_n is vanishingly low, the shell gap at $N=82$ merges into the continuum. Consequently, the ensuing shell structure above $N=82$ is washed out significantly. Since a nucleus cannot take on any more neutrons, nuclei in the vicinity of the drip line are, therefore, not expected to contribute to the r-process nucleosynthesis.

ACKNOWLEDGMENTS

[1] K.-L. Kratz, J.P. Bitouzet, F.K. Thielemann, P. Möller, and B. Pfeiffer, Astrophys. J. **403**, 216 (1993).

[2] M.M. Sharma, G.A. Lalazissis, W. Hillebrandt, and P. Ring, Phys. Rev. Lett. **72**, 1431 (1994); **73**, 1870 (1994).

[3] J. Dobaczewski, I. Hamamoto, W. Nazarewicz, and J.A. Sheikh, Phys. Rev. Lett. **72**, 981 (1994).

[4] M.M. Sharma, A.R. Farhan, and S. Mythili, Phys. Rev. C **61**, 054306 (2000).

[5] C. Borcea *et al.*, Nucl. Phys. **A565**, 158 (1993).

[6] M.G. Mayer and J.H.D. Jensen, *Elementary Theory of Nuclear Structure* (Wiley, New York, 1955).

[7] B.D. Serot and J.D. Walecka, Adv. Nucl. Phys. **16**, 1 (1986).

[8] M.M. Sharma, G.A. Lalazissis, and P. Ring, Phys. Lett. B **317**, 9 (1993).

[9] M.M. Sharma, G.A. Lalazissis, J. König, and P. Ring, Phys. Rev. Lett. **74**, 3744 (1994).

[10] A.R. Bodmer, Nucl. Phys. **A526**, 703 (1991).

[11] L.P. Gorkov, Zh. Éksp. Teor. Fiz. **34**, 735 (1958) [Sov. Phys. JETP **7**, 505 (1958)].

[12] H. Kucharek and P. Ring, Z. Phys. A **339**, 23 (1991).

[13] J.F. Berger, M. Girod, and D. Gogny, Nucl. Phys. **A428**, 32 (1984).

[14] Y.K. Gambir, P. Ring, and A. Thimet, Ann. Phys. (N.Y.) **198**, 132 (1990).

[15] M.M. Sharma, M.A. Nagarajan, and P. Ring, Phys. Lett. B **312**, 377 (1993).

[16] G.A. Lalazissis, J. König, and P. Ring, Phys. Rev. C **55**, 540 (1997).

[17] M.M. Sharma (unpublished).

[18] G. Audi and A.H. Wapstra, Nucl. Phys. **A595**, 409 (1995).

[19] J. Dobaczewski, H. Flocard, and J. Treiner, Nucl. Phys. **A422**, 103 (1984).

[20] P.G. Reinhard, Rep. Prog. Phys. **52**, 439 (1989).

[21] M.M. Sharma, M.A. Nagarajan, and P. Ring, Ann. Phys. (N.Y.) **231**, 110 (1994).

[22] B. Chen, J. Dobaczewski, K.-L. Kratz, K. Langanke, B. Pfeifer, F.-K. Thielemann, and P. Vogel, Phys. Lett. B **355**, 37 (1995).